Total reaction cross sections for ^{8}Li + ^{90}Zr at near-barrier energies

A. Pakou[1,a], D. Pierroutsakou[2], M. Mazzocco[3,4], L. Acosta[5], X. Aslanoglou[1], A. Boiano[2], C. Boiano[6], D. Carbone[7], M. Cavallaro[7], J. Grebosz[8], N. Keeley[9], M. La Commara[10,2], C. Manea[4], G. Marquinez-Duran[5], I. Martel[5], C. Parascandolo[2], K. Rusek[11], A. M. Sánchez-Benítez[12], O. Sgouros[1], C. Signorini[13], F. Soramel[3,4], V. Soukeras[1], E. Stiliaris[14], E. Strano[3,4], D. Torresi[3,4], A. Trzcinska[11], Y. X. Watanabe[15], and H. Yamaguchi[16]

[1] Department of Physics and HINP, The University of Ioannina, 45110 Ioannina, Greece
[2] INFN, Sezione di Napoli, via Cintia, 80126 Napoli, Italy
[3] Dipartimento di Fisica e Astronomia, Università di Padova, via Marzolo 8, I-35131, Padova, Italy
[4] INFN, Sezione di Padova, via Marzolo 8, I-35131, Padova, Italy
[5] Departamento de Fisica Aplicada, Universidad de Huelva E-21071 Huelva, Spain
[6] INFN, Sezione di Milano, via Celoria 16, I-20133 Milano, Italy
[7] INFN Laboratori Nazionali del Sud, via S. Sofia 62, 95125, Catania, Italy
[8] The Henryk Niewodniczanski Institute of Nuclear Physics (IFJ PAN), Krakow, Poland
[9] National Center for Nuclear Research, A. Soltana 7, 05-400, Otwock Warsaw, Poland
[10] Dipartimento di Scienze Fisiche, Università di Napoli "Federico II", via Cintia, I-80126 Napoli, Italy
[11] Heavy Ion Laboratory, University of Warsaw, Pasteura 5a, 02-093, Warsaw, Poland
[12] Centro de Física Nuclear da Universidade de Lisboa, 1649-003 Lisboa, Portugal
[13] INFN, LNL, viale dell'Università 2, I-35020 Legnaro, Italy
[14] Institute of Accelerating Systems and Applications and Department of Physics, University of Athens, Greece
[15] Institute of Particle and Nuclear Studies (IPNS), High Energy Accelerator Research Organization (KEK), Tsukuba, 305-0801 Ibaraki, Japan
[16] Center for Nuclear Study (CNS), University of Tokyo, RIKEN campus, 2-1 Hirosawa, Wako, Saitama 351-0198, Japan

Abstract. Total reaction cross sections for the radioactive nucleus ^{8}Li on ^{90}Zr are reported at the near-barrier energies of 18.5 and 21.5 MeV, derived from quasi-elastic scattering measurements. An analysis of the quasi-elastic scattering results is performed within an optical model framework using the BDM3Y1 interaction and total reaction cross sections are deduced. These quantities, appropriately reduced, are compared with previous data obtained in elastic scattering measurements with well and weakly bound projectiles on various targets and a formula for predicting total reaction cross sections with an uncertainty of $\sim 20\%$ is obtained. Further on, the ratios of direct to total reaction cross sections are estimated for ^{6,8}Li on various targets and are compared with CDCC or CRC calculations. The energy dependence of the optical potential is also discussed.

1 Introduction

The merit of channel coupling effects for understanding the structure of projectile and target nuclei in the vicinity of the Coulomb barrier is indisputable. The effects on the elastic scattering for stable nuclei may be strong [1, 2], while they can be even more striking for radioactive beams [3, 4]. Large transfer/breakup cross sections persist to very low energies —even below the barrier— for light weakly bound projectiles on heavy [5], medium [6] and light targets [7, 8]. Elastic scattering is then the tool for tracing such effects.

We present here the results of an optical model analysis of the quasi-elastic scattering for ^{8}Li + ^{90}Zr at two energies, 18.5 and 21.5 MeV (energies in the middle of the target), that complement a recent study [9] where the data were analyzed in the coupled reaction channels (CRC) framework. The analysis is performed in a BDM3Y1 framework and the energy dependence of the optical potential, directly connected to the channel coupling

[a] e-mail: apakou@cc.uoi.gr

effects, is discussed. The main goal of this work, however, concerns total reaction cross sections, which are deduced and considered in a systematics involving tightly bound (^{16}O, ^{12}C [10–14]), weakly bound stable (^{6,7}Li [2, 15–19]) and the weakly bound radioactive projectiles ^{8}Li and ^{6}He on light and medium mass targets (^{27}Al, ^{58}Ni, ^{64}Zn, ^{90}Zr —the present work and refs. [6, 20, 21]) as well as on the heavier target ^{208}Pb [5, 22, 23].

In order to perform systematic studies of total reaction cross sections in collisions of weakly bound nuclei *versus* well bound ones, it is necessary to reduce the data according to some procedure and compare them to some benchmark as is very well stated in ref. [24]. As the most promising, we have chosen the procedure described in refs. [25–27], where the results were reduced according to the Wong formula. This technique was first applied to fusion excitation functions and the reduced results were called "fusion functions". The representation of fusion functions for various projectiles on various targets at near-barrier energies gave self-consistent results and the universal fusion function (uff), a reduced function according to the Wong formula for fusion cross sections, was derived. Deviations from the uff below the barrier were interpreted as due to channel coupling effects. This technique will be applied here to total reaction cross sections according to [28] and a formula —a best fit reaction function to the experimental results— will be given for predicting total reaction cross sections at near-barrier energies. A comparison of this total reaction function with the universal fusion function will give an estimate of the importance of direct reaction channels.

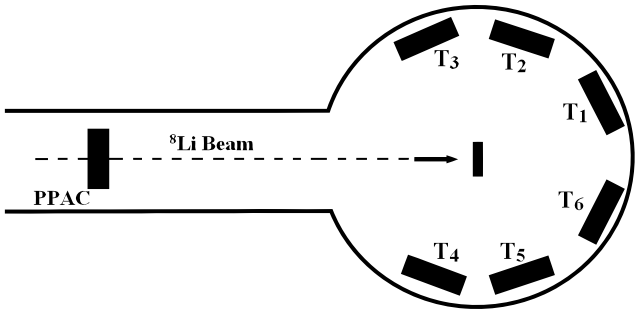

Fig. 1. Experimental setup with the EXOTIC facility detector array, described in [30], including 6 telescopes in the present experiment.

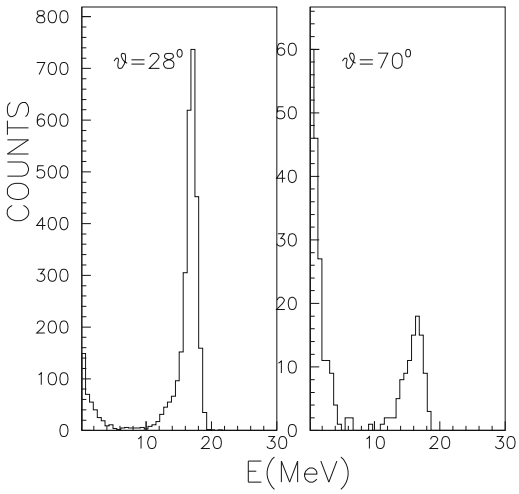

Fig. 2. Particle spectra obtained in the reaction ^{8}Li + ^{90}Zr at incident energy of 18.9 MeV at forward and backward angles (forward and middle telescopes). It should be noted that the quasi-elastic scattered lithium particles stop in the first stage of the telescopes. The main observed peak corresponds to quasi-elastic scattering.

2 Experimental details

The ^{8}Li secondary beam was produced at the EXOTIC facility [29] at the Laboratori Nazionali di Legnaro (LNL), Italy by means of the in-flight (IF) technique and the ^{2}H(^{7}Li, ^{8}Li)p reaction ($Q_{\rm val} = -0.19$ MeV). The ^{7}Li^{+3} primary beam was delivered by the LNL-XTU Tandem Van de Graaf accelerator with an intensity of ~ 150 pnA and at energies of 27 and 29 MeV. It was directed onto a 5 cm long gas cell with 2.2 μm thick Havar foil windows filled with ^{2}H gas at a pressure of 1217 mbar and a temperature of 93 K, corresponding to an effective thickness of 2 mg/cm^2. A parallel plate avalanche counter (PPAC) was placed downstream 88 cm before the secondary target and used to monitor the beam. Beam purity optimization was achieved by recording the energy spectrum of the secondary beam in different Si detectors placed across the EXOTIC beam line. Further details of the beam production are given in ref. [9].

Our experimental setup included six telescopes from the detector array of the EXOTIC facility described in [30] and is presented schematically in fig. 1. Each telescope is comprised of ΔE and E double-sided silicon strip detectors, with thicknesses $\sim 55\,\mu$m and $300\,\mu$m, respectively. Both modules have active areas of 64×64 mm^2 with 32 strips per side, orthogonally oriented to define 2×2 mm^2 pixels. Details of handling the detector signals can be found in ref. [30]. At the lower energy, the elastically scattered ejectiles were detected in the first stage of the telescope, where they stopped. A particle spectrum is presented in fig. 2, for a forward and a backward angle. At the higher energy and in the forward detectors the elastically scattered ejectiles were well discriminated from other particles by the ΔE-E technique. Due to some problems with the middle detectors, data at the projectile energy of 21.5 MeV were not collected in the angular range $\theta_{\rm lab} = 69^\circ \pm 16^\circ$. The telescopes were fixed at a distance of ~ 11 cm from the target position covering a total solid angle of ~ 1.7 sr. The strips were short-circuited two by two, therefore the angular resolution is in principle $\sim 2^\circ$ per angular position, considering a point-like beam spot on target. However, taking into account that the beam spot on target should have diameter ~ 10 mm, according to previous studies [31], and the finite dimensions of a "double" strip, the actual angular resolution is estimated to be at most 5 degrees. A ^{90}Zr target of thickness 1.5 mg/cm^2

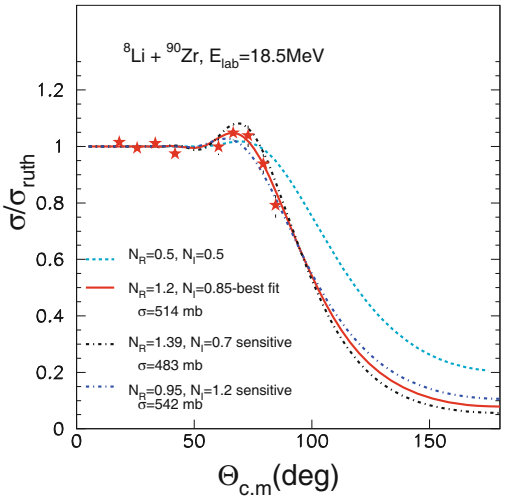

Fig. 3. Present experimental data on the quasi-elastic scattering of ^{8}Li + ^{90}Zr at 18.5 MeV (middle of the target), analyzed within an optical model framework with double-folded potentials based on the BDM3Y1 interaction. The best fit normalization factors of the real and imaginary parts of the optical potential are given on the figure. The dashed curve denotes the result for conventional values for weakly bound stable systems.

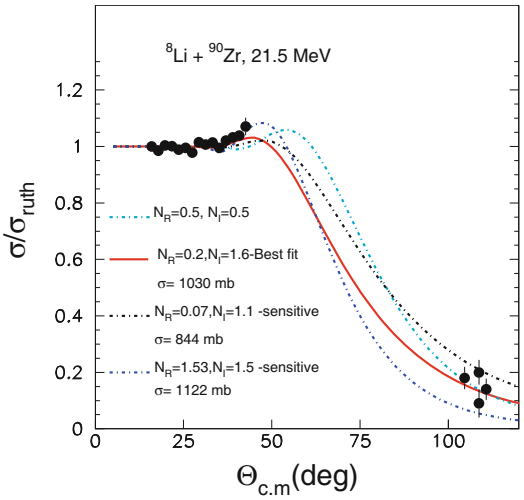

Fig. 4. Same as in fig. 3 but for projectile energy $E_{\rm lab}$ = 21.5 MeV (middle of the target). It should be noted that the data points at forward angles originate from an analysis using the ΔE-E technique for resolving the quasi-elastic scattering of ^{8}Li. This is not true for the 4 backward data points, where the ejectiles stop in the first stage of the telescope.

was installed in a target ladder at the center of the target chamber, perpendicular to the beam. A ^{208}Pb target, 2 mg/cm^2 thick, was installed on the same ladder, and was used in a subsequent run to deduce the solid angle by assuming that the elastic scattering over the whole angular range was described by the Rutherford formula. For the reduction of the data, a pixel analysis was performed after an appropriate angle assignment was done geometrically in each pixel.

3 Data reduction and optical model analysis

In figs. 3 and 4 we present our experimental results which refer to quasi-elastic scattering due to the unresolved inelastic excitations. The differential quasi-elastic scattering cross sections *versus* Rutherford scattering were obtained using the following relation:

$$\frac{\sigma(\theta)}{\sigma_{\rm Ruth}(\theta)} = \frac{N(\theta)\sigma^{\rm Pb}_{\rm Ruth}(\theta)\Phi_{\rm Pb}T_{\rm Pb}}{N_{\rm Pb}(\theta)\sigma_{\rm Ruth}(\theta)\Phi T}\,, \qquad (1)$$

where $\sigma(\theta)$ is the differential cross section for the ^{8}Li + ^{90}Zr quasi-elastic scattering at 18.5 MeV or 21.5 MeV, $N(\theta)$ is the quasi-elastic scattering counting rate for ^{8}Li on ^{90}Zr, $\sigma^{\rm Pb}_{\rm Ruth}(\theta)$ and $\sigma_{\rm Ruth}(\theta)$ is the Rutherford scattering differential cross section for ^{8}Li on the ^{208}Pb and ^{90}Zr targets, respectively, $\Phi_{\rm Pb}$ is the beam flux during the run with the ^{208}Pb target, $N_{\rm Pb}(\theta)$ is the counting rate for the ^{208}Pb run at the same angle as with the ^{90}Zr target, Φ is the beam flux during the run with the ^{90}Zr target, and finally $T_{\rm Pb}$ and T are the ^{208}Pb and ^{90}Zr target thicknesses, respectively. The quantity $(\Phi_{\rm Pb}T_{\rm Pb})/(\Phi T)$ was adjusted such that at the most forward angles the ratio of the cross section to Rutherford was equal to 1.0. In this way the assigned error on our data is mostly due to the statistical error. It should be noted that due to the lower statistics of the 18.5 MeV run and taking into account the angular resolution of ~ 5 degrees, differential cross sections appearing in fig. 3 are the weighted means every three scattering angles. It should be also noted that the quasi-elastic scattering obtained in this work, instead of pure elastic, does not affect our results as according to preliminary calculations for ^{8}Li + ^{90}Zr, inelastic excitation is negligible. The same result was found before for inelastic excitation of ^{8}Li + ^{208}Pb in ref. [5] for near-barrier energies.

In order to obtain the energy dependence of the optical potential and to deduce total reaction cross sections, the data were analyzed in an optical model framework, using a double-folded potential calculated with the BDM3Y1 interaction [32] for both the real and imaginary parts. The ^{90}Zr matter density was derived from the nuclear charge density of ref. [33] by unfolding the proton charge distribution and making the isoscalar assumption, $\rho_{\rm Nuc} = 1 + (N/Z)\rho_p$, while the ^{8}Li density was derived from ref. [34]. The differential cross sections were obtained using the code ECIS [35] and the best fit normalization factors for the real and imaginary parts of the optical potential were deduced via a χ^2 minimization procedure. The adopted errors in these values were deduced from a sensitivity analysis, performed by varying the parameters N$_R$ and N$_I$ by certain amounts. The obtained fits to the distributions are designated as "sensitive" for the sensitivity analysis and best for the best fit in figs. 3 and 4. The obtained total reaction cross sections from this analysis are (514 ± 30) mb and (1030 ± 140) mb for the 18.5 and the 21.5 MeV energies, respectively. The assigned errors are related with the obtained cross sections in the sensitivity analysis described above, where only the statistical error

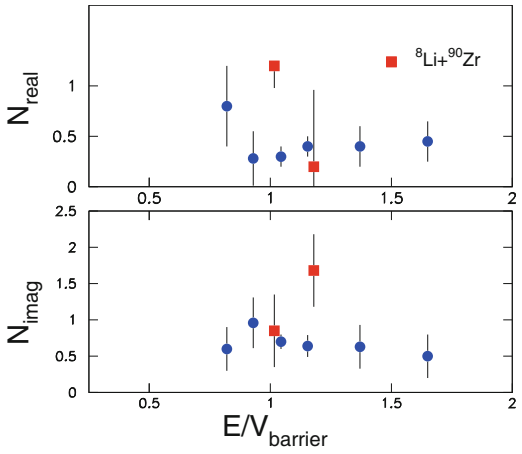

Fig. 5. Energy dependence of the optical potential for $^{8}\mathrm{Li} + {}^{90}\mathrm{Zr}$ extracted from the present quasi-elastic scattering data, compared with results for $^{6}\mathrm{Li} + {}^{90}\mathrm{Zr}$, extracted from previous elastic scattering data [18]. Both data sets were analyzed within the same BDM3Y1 framework.

is taken into account. If we increase this error to $\sim 10\%$ in order to include other systematic errors, then the assigned uncertainty to the cross sections is estimnated to be doubled.

Further on, the results of the obtained potential parameters are presented in fig. 5, and are compared with results for $^{6}\mathrm{Li} + {}^{90}\mathrm{Zr}$. The latter were obtained within the same BDM3Y1 framework, using the ^{6}Li density from ref. [36] and previously measured elastic scattering data from ref. [18].

4 Systematics of total reaction cross sections

As mentioned in the introduction, we have adopted the same reduction procedure as suggested in ref. [25] for fusion cross sections. In more detail, Wong obtained the following analytic expression for the fusion cross section, approximating the barrier by a parabola (an inverted harmonic oscillator potential) and neglecting the variation of the barrier radius with angular momentum:

$$\sigma_{\mathrm{F}}^{\mathrm{W}} = R_{\mathrm{B}}^{2}\,\frac{\hbar\omega}{2E_{\mathrm{c.m.}}}\,\ln\left[1+\exp\left(\frac{2\pi(E_{\mathrm{c.m.}}-V_{\mathrm{B}})}{\hbar\omega}\right)\right], \quad (2)$$

where $(\hbar\omega)$, (R_{B}) and (V_{B}) are the curvature, radius and height of the potential, respectively. In this scheme the fusion cross section, σ_{F}, and the energy, $E_{\mathrm{c.m}}$, of the projectile can be reduced using the following formulas:

$$\sigma_{\mathrm{F}} \rightarrow F(x) = \frac{2E_{\mathrm{c.m.}}}{\hbar\omega R_{\mathrm{B}}^{2}}\sigma_{\mathrm{F}}, \quad (3)$$

corresponding to an energy in the center of mass, $E_{\mathrm{c.m}}$, reduced to the quantity x given by the equation

$$E_{\mathrm{c.m.}} \rightarrow x = \frac{E_{\mathrm{c.m.}} - V_{\mathrm{B}}}{\hbar\omega}\,. \quad (4)$$

Table 1. Potential properties: barrier V_{B}, radius R_{B} and curvature $\hbar\omega$.

System	V_{B} (MeV)	R_{B} (fm)	$\hbar\omega$ (MeV)
$^{8}\mathrm{Li} + {}^{90}\mathrm{Zr}$	16.464	9.801	3.639
$^{6}\mathrm{Li} + {}^{90}\mathrm{Zr}$	17.051	9.435	4.283
$^{12}\mathrm{C} + {}^{90}\mathrm{Zr}$	32.615	9.888	4.152
$^{16}\mathrm{O} + {}^{90}\mathrm{Zr}$	42.615	10.099	4.105
$^{6}\mathrm{Li} + {}^{28}\mathrm{Si}$	7.008	7.931	3.226
$^{7}\mathrm{Li} + {}^{28}\mathrm{Si}$	6.840	8.147	2.963
$^{6}\mathrm{Li} + {}^{27}\mathrm{Al}$	6.512	7.927	3.123
$^{6}\mathrm{He} + {}^{27}\mathrm{Al}$	4.201	8.222	2.487
$^{6}\mathrm{Li} + {}^{58}\mathrm{Ni}$	12.788	8.759	3.927
$^{6}\mathrm{He} + {}^{58}\mathrm{Ni}$	8.274	9.056	3.150
$^{6}\mathrm{Li} + {}^{64}\mathrm{Zn}$	12.788	8.759	3.927
$^{6}\mathrm{He} + {}^{64}\mathrm{Zn}$	8.742	9.194	3.197
$^{6}\mathrm{Li} + {}^{120}\mathrm{Zr}$	20.282	9.948	4.507
$^{8}\mathrm{Li} + {}^{208}\mathrm{Pb}$	29.364	11.365	4.357
$^{6}\mathrm{Li} + {}^{208}\mathrm{Pb}$	30.178	11.035	5.125
$^{7}\mathrm{Li} + {}^{208}\mathrm{Pb}$	29.743	11.209	4.699
$^{6}\mathrm{He} + {}^{208}\mathrm{Pb}$	19.780	11.247	4.176
$^{12}\mathrm{C} + {}^{208}\mathrm{Pb}$	58.071	11.483	4.873
$^{16}\mathrm{O} + {}^{208}\mathrm{Pb}$	76.083	11.689	4.755

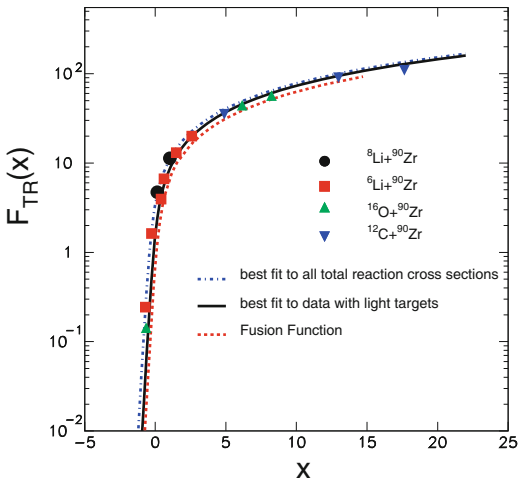

Fig. 6. Present data for the $^{8}\mathrm{Li} + {}^{90}\mathrm{Zr}$ total reaction cross section, reduced according to ref. [25], compared with previous data [11–13, 18] for the weakly bound but stable projectile ^{6}Li and the well bound projectiles ^{12}C and ^{16}O on the same target, ^{90}Zr. The dot-dashed blue line represents the best fit to the group of all data sets considered in this work (see text) while the solid black line is the best fit to data for the light targets (^{27}Al and ^{28}Si). The dashed red line represents the universal fusion function (uff).

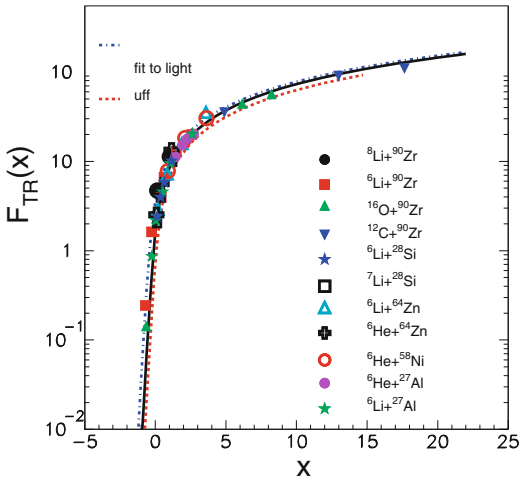

Fig. 7. Same as in fig. 6 but for several light and medium mass targets and with the additional neutron rich radioactive projectile ^{6}He.

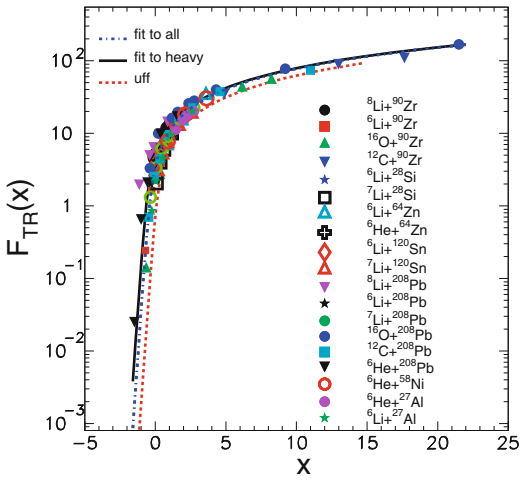

Fig. 8. Same as in figs. 6 and 7 but including various targets from mass number $A = 27$ to 208. Previous data are from [2, 5, 6, 10–23].

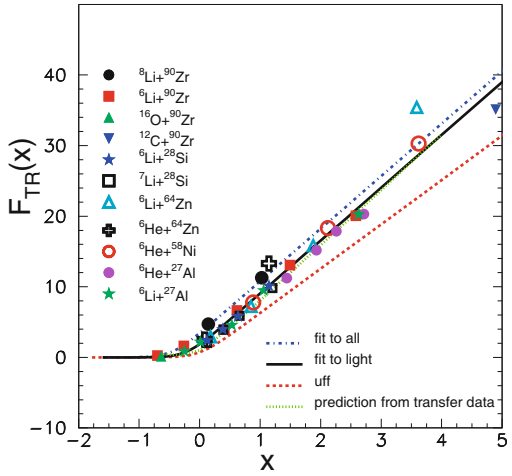

Fig. 9. As in fig. 7 but showing on a linear scale the lower energy data. The dotted green line represents the results of previous CDCC calculations for ^{6}Li + ^{28}Si [7,8] which describe well the experimental data displayed as a ratio of the transfer to total reaction cross section. See also fig. 13 and text.

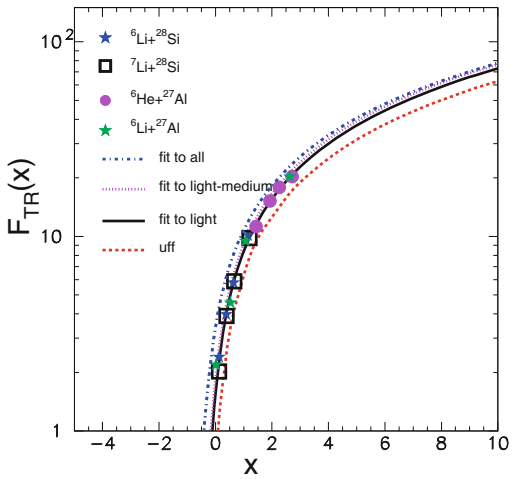

Fig. 10. As in figs. 6, 7, and 8 but for the light targets ^{27}Al and ^{28}Si.

According to the above relations and replacing $\sigma_{\rm F}$ with $\sigma_{\rm R}$ as in [28] (fusion with reaction cross section) total reaction cross section functions as a function of x, F$_{TR}$(x), were formed for all data. Curvatures ($\hbar\omega$), radii ($R_{\rm B}$) and potential heights ($V_{\rm B}$) were deduced using the Christensen-Winther potential [37] and the values obtained are included in table 1. The reduced total reaction cross sections for selected previously studied systems and the present results are presented in figs. 6, 7, 8, 9 (on a linear scale), 10 and 11. It should be noted that for reasons of inter-consistency all previous elastic scattering data, with the exception of ^{6,7,8}Li + ^{208}Pb, were reanalyzed in the same BDM3Y1 framework as the present data, and total reaction cross sections were deduced and reduced accordingly. The results for weakly bound stable and radioactive projectiles (^{6,8}Li) are compared with the results for stable projectiles (^{12}C, ^{16}O) on the same target, ^{90}Zr, in more detail in fig. 6. They exhibit in principle rather similar behavior within an uncertainty band of $\sim$ 10 to 15%. However, the results do not span a uniform energy range, thus preventing any further strong conclusions. For a more global perception we present in fig. 7 the results for the same projectiles and ^{7}Li and ^{6}He on light and medium mass targets from ^{27}Al to ^{90}Zr. The conclusions from fig. 6 are also valid for the results in fig. 7. In fig. 8 we present the results for the same projectiles but including the heavy target ^{208}Pb and in figs. 10 and 11, respectively, data for light and heavy targets separately. In fig. 9 results at lower energies for light and medium mass targets are presented on a linear scale, for reasons of clarity. It is obvious that the best agreement occurs for total reaction cross sections on the same target, irrespective of whether the projectile is well or weakly bound. When data for various projectiles on various targets are presented, the uncertainty band is as large as $\sim$ 20%. Taking into account, however, that the

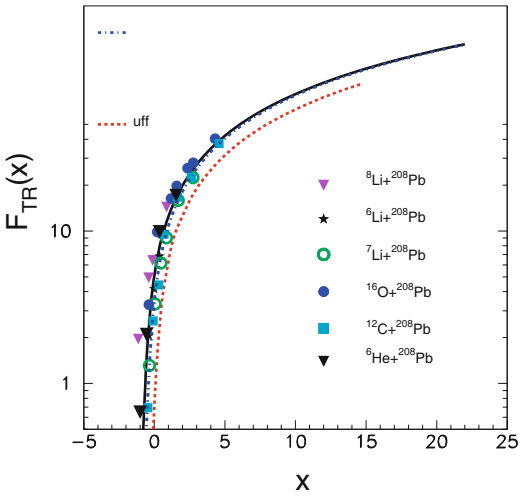

Fig. 11. As in figs. 6, 7, 8 but for the heavy target ^{208}Pb.

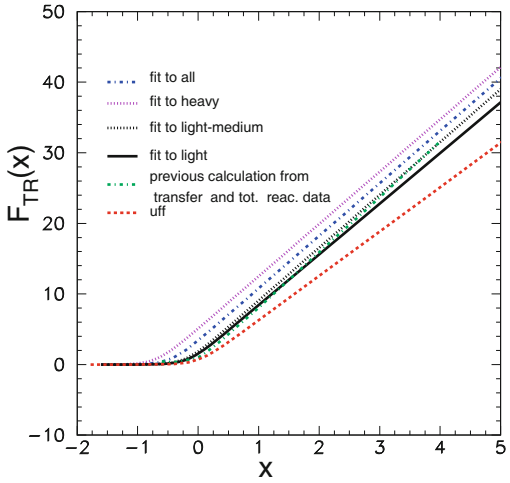

Fig. 12. Comparison of best fits to total reaction cross section data reduced according to the Wong cross section [25], $F_{TR}(x)$, with the uff and a total reaction cross section function deduced from previous transfer data on ^{6}Li + ^{28}Si, see text.

uncertainty on every datum is usually of the order of 10%, at least for measurements around the barrier, then we are entitled to use this representation as a guide for estimates of the total reaction cross section. To that end we have performed a best fit using the following relation with two free parameters, a and b:

$$Y(x) = a \ln\left[1 + \exp(2\pi x - b)\right]. \qquad (5)$$

The best fit values for all data sets from $A = 27$ to 208 were $a = 1.18406$ and $b = -2.83337$, for light targets only (^{28}Si and ^{27}Al) $a = 1.14409$, $b = -1.06089$, for the heavy target ^{208}Pb only $a = 1.17937$, $b = -4.31818$ and finally for light medium mass targets from $A = 27$ to $A = 90$ $a = 1.19116$, $b = -1.32898$. The results are shown in figs. 6, 7, 8, 9, 10 and 11 and are compared amongst themselves in fig. 12. Moreover all results are compared with the universal fusion function (uff) defined in ref. [25]

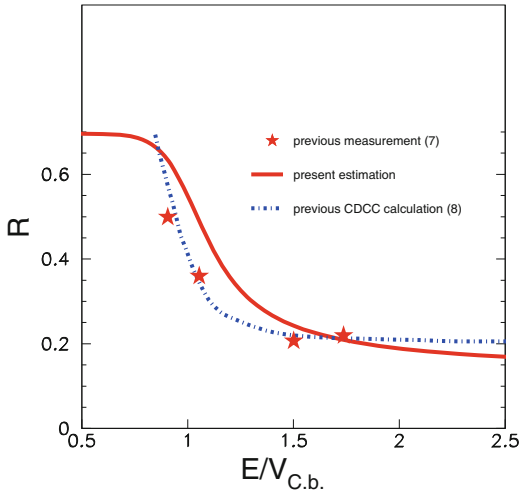

Fig. 13. The quantity R, the ratio of direct to total reaction cross section, as a function of energy *versus* the Coulomb barrier according to Broglia [40], for ^{6}Li + ^{28}Si. The data and the CDCC calculations, denoted by the dot-dashed blue line, are from refs. [7] and [8], respectively, while the solid red line represents the present estimate.

via the relation

$$F_0(x) = \ln[1 + \exp(2\pi x)] \qquad (6)$$

and denoted in the figures by a dashed red line. The difference between this line and the best fit

$$R = \frac{Y(x) - \mathrm{F_0(x)}}{Y(x)}\,. \qquad (7)$$

gives in principle the contribution of direct channels to the reaction process at least an upper limit, as for the uff ($F_0(x)$) no coupling effects are considered.

This difference is quantified in fig. 13 for ^{6}Li + ^{28}Si, as a ratio of direct to total reaction cross section and compared with Continuum Discretized Coupled-Channels (CDCC) calculation and experimental results measured previously [7, 8]. To obtain reaction cross section in the CDCC framework we note that the elastic scattering can be well reproduced by simple optical model calculations, where the effective potential is described as a sum of a bare potential and a dynamic polarization potential. The dynamic polarization potential, generated by the breakup of the lithium in the field of the silicon target, is derived from CDCC calculations following the prescription of Thompson [38]. It is assumed that ^{6}Li has a simple two-body alpha+d cluster structure and couplings with the resonant and non-resonant states of alpha+d continuum are taken into account. The elastic scattering calculations based on this optical potential reproduce very well the ^{6}Li + ^{28}Si elastic scattering data [16] as well as breakup cross section data [39] with no free parameters. The cross section due to direct channels, σ_D, was extracted from magnitudes obtained in the above calculation that is, the total reaction cross section, σ_T, and fusion cross section, σ_F, as $\sigma_D = \sigma_T$-σ_F. Subsequently the ratio R was derived as

$R = \sigma_D/\sigma_T$. The agreement between the prediction and experimental and theoretical results is good to within an uncertainty of at most $\sim 15\%$. It is remarkable that the present estimate of this ratio was made taking into account a fit to the reduced total reaction cross sections for light targets (black curve in fig. 12) and the universal fusion function (uff): In this respect this estimate gives an upper limit to the ratio of direct to total reaction cross section, underling the view that fusion is a simple process which can be described by a single barrier penetration theory (Wong here) with some deviations due to channel coupling effects. However, in order to probe these effects precise measurements are required, something which is not the case for the available total reaction cross section data below and/or near the Coulomb barrier.

In addition, in the same context but in a vice versa procedure than the above, we have calculated the total reaction cross section function for $^{6}\mathrm{Li} + {}^{28}\mathrm{Si}$ from ratios determined experimentally and theoretically previously (see fig. 13) and the uff function, applying eq. (7). The result is shown as the dashed green line in figs. 9 and 12. The agreement with the solid black line which comes from the best fit to the total reaction cross section data obtained with light targets (^{27}Al and ^{28}Si) is remarkable. It is even more remarkable that, as demonstrated in fig. 9, the reduced data for either stable or radioactive projectiles such as ^{6}He are gathered around the same line, with the greatest deviations observed for ^{6}He and ^{8}Li incident on the heavier targets (^{64}Zn and ^{90}Zr). In other words, total reaction cross sections for the same or similar targets, when they are deduced in the same theoretical framework and are appropriately reduced, present the same behavior —into the experimental uncertainty— irrespective of whether the projectile is weakly bound or not.

In fig. 14 our estimates via eq. (7) for the direct to total ratio for ^{8}Li on various targets are presented. While these ratios are given as upper limits, the comparison for the various targets is interesting, especially at the lower energies where saturation occurs. This saturation value approaches unity for a lead target and it will be very interesting to see in a future measurement the result of channel coupling effects. In the same figure, coupled reaction channel (CRC) calculations for $^{8}\mathrm{Li} + {}^{90}\mathrm{Zr}$ and $^{8}\mathrm{Li} + {}^{208}\mathrm{Pb}$ are also shown, presenting a good agreement with our present estimation. CRC calculations for $^{8}\mathrm{Li} + {}^{90}\mathrm{Zr}$ system were identical to those of ref. [9] with the exception that the $^{90}\mathrm{Zr}(^{8}\mathrm{Li}, {}^{9}\mathrm{Be})^{89}\mathrm{Y}$ single proton pickup couplings were omitted since they had a negligible effect on both the elastic scattering and the summed direct reaction cross section. Similar calculations were also performed for the $^{8}\mathrm{Li} + {}^{208}\mathrm{Pb}$ system taking the nuclear matter densities, exit channel optical potentials, etc., from the same sources. The spectroscopic factors for the $\langle {}^{209}\mathrm{Pb}|{}^{208}\mathrm{Pb} + n\rangle$ overlaps were taken from ref. [42]. The observed small deviations of these calculations and our estimation should be due to coupling channel effects not taken into account in our fusion calculation (Wong calculation). As the deviations are small, it becomes evident from this comparison, that for ^{8}Li, coupling channel effects are not strong.

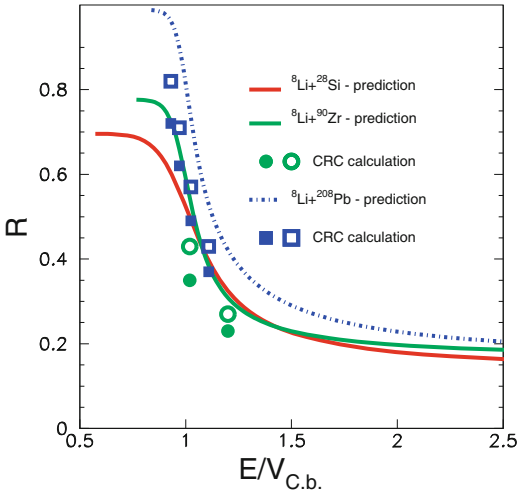

Fig. 14. Ratios of direct to total reaction cross section for ^{8}Li on various targets, estimated using the total reaction cross section systematics and the uff. The predictions are compared with CRC calculations, performed with two different densities, according to ref. [34] —closed symbols— and [41] —open symbols—.

5 Summary and conclusions

We have measured quasi-elastic scattering angular distributions for the radioactive projectile ^{8}Li on a ^{90}Zr target at two near-barrier energies, 18.5 and 21.5 MeV ($V_{\mathrm{C.b.}}^{\mathrm{lab}} = 18.21$ MeV). The results were analyzed within an optical model framework and total reaction cross sections were deduced. The new results were considered in a systematics by reanalyzing in the same framework previous results on light, medium and heavy targets with the following conclusions. Total reaction cross sections for stable or weakly bound projectiles on the same or similar targets, reduced according to the Wong formula in the prescription of refs. [25, 28], present similar behavior with some small deviations close to and below the barrier, possibly due to channel coupling effects. Into this context, prediction formulas for total reaction cross sections are suggested within an uncertainty band of 20%. Fusion is a simple procedure obeying in principle a single barrier penetration theory with deviations of second order which, in order to be traced, require cross section measurements with very small uncertainties. Moreover ratios of direct processes to total reaction cross sections are also predicted with very interesting results. That is, in general, these ratios underline the fact that direct processes are major contributors to the total reaction cross section for incident energies near the Coulomb barrier and become even more important below the barrier. This contribution is larger for the heavier targets, where direct processes tend to exhaust almost all the total reaction cross section below barrier. The conclusions from the optical potential energy dependence as obtained in this work is not clear, as it includes only two data points with large uncertainties. However the indication is that for ^{8}Li the absorption from the elastic channel is very large, and indeed larger than

that exhibited by the weakly bound but stable projectile ^{6}Li. With some cautious we could also say that for ^{8}Li the imaginary potential drops at barrier and this reduction is connected with an increase of the real part, resembling the behavior of well bound nuclei. More data are necessary to confirm this last conclusion.

We would like to acknowledge warmly Massimo Loriggiola from Laboratori Nationali di Legnaro for providing the zirconium targets and, in fact, in a very short notice of time. The research leading to these results has received funding partly from the European Union Seventh Framework Programme FP7/2007-2013 under Grant Agreement No. 262010-ENSAR.

References

1. C.E. Thorn, M.J. LeVine, J.J. Kolata, C. Flaum, P.D. Bond, J.C. Sens, Phys. Rev. Lett. **38**, 384 (1977).
2. N. Keeley, S.J. Bennett, N.M. Clarke, B.R. Fulton, G. Tungate, P.V. Drumm, M.A. Nagarajan, J.S. Lilley, Nucl. Phys. A **571**, 326 (1994).
3. N. Keeley, N. Alamanos, K.W. Kemper, K. Rusek Prog. Part. Nucl. Phys. **63**, 396 (2009).
4. N. Keeley, J. Phys. Conf. Ser. C **381**, 012087 (2012).
5. J.J. Kolata, V.Z. Goldberg, L.O. Lamm, M.G. Marino, C.J. O'Keeffe, G. Rogachev, E.F. Aguilera, H. Garcia-Martinez, E. Martinez-Quiroz, P. Rosales, F.D. Becchetti, T.W. O'Donnell, D.A. Roberts, J.A. Brown, P.A. DeYoung, J.D. Hinnefeld, S.A. Shaheen, Phys. Rev. C **65**, 054616 (2002).
6. A. Di Pietro, P. Figuera, F. Amorini, C. Angulo, G. Cardella, S. Cherubini, T. Davinson, D. Leanza, J. Lu, H. Mahmud, M. Milin, A. Musumarra, A. Ninane, M. Papa, M.G. Pellegriti, R. Raabe, F. Rizzo, C. Ruiz, A.C. Shotter, N. Soic, S. Tudisco, L. Weissman, Phys. Rev. C **69**, 044613 (2004).
7. A. Pakou, K. Rusek, N. Alamanos, X. Aslanoglou, S. Harissopulos, M. Kokkoris, A. Lagoyannis, T.J. Mertzimekis, A. Musumarra, N.G. Nicolis, C. Papachristodoulou, D. Pierroutsakou, D. Roubos, Phys. Rev. C **76**, 054601 (2007).
8. A. Pakou, K. Rusek, N. Alamanos, X. Aslanoglou, M. Kokkoris, A. Lagoyannis, T.J. Mertzimekis, A. Musumarra, N.G. Nicolis, D. Pierroutsakou, D. Roubos, Eur. Phys. J. A **39**, 187 (2009).
9. A. Pakou *et al.*, submitted to Phys. Lett. B.
10. S. Santra, P. Singh, S. Kailas, A. Chatterjee, A. Shrivastava, K. Mahata, Phys. Rev. C **64**, 024602 (2001).
11. S.T. Thornton, D.E. Gustafson, J.L.C. Ford, Jr., K.S. Toth, D.C. Hensley, Phys. Rev. C **13**, 1502 (1976).
12. P.P. Tung, K.A. Erb, M.W. Sachs, G. B. Sherwood, R.J. Ascuitto, D.A. Bromley, Phys. Rev. C **18**, 1663 (1978).
13. M.A.G. Alvarez, L.C. Chamon, D. Pereira, E.S. Rossi Jr., C.P. Silva, L.R. Gasques, H. Dias, M.O. Roos, Nucl. Phys. A **656**, 187 (1999).
14. F. Videbaek, R.B. Goldstein, L. Grodzins, S.G. Steadman, T.A. Belote, J.D. Garrett, Phys. Rev. C **15**, 954 (1977).
15. A. Pakou, N. Alamanos, G. Doukelis, A. Gillibert, G. Kalyva, M. Kokkoris, S. Kossionides, A. Lagoyannis, A. Musumarra, C. Papachristodoulou, N. Patronis, G. Perdikakis, D. Pierroutsakou, E.C. Pollacco, K. Rusek, Phys. Rev. C **69**, 054602 (2004).
16. A. Pakou, N. Alamanos, A. Lagoyannis, A. Gillibert, E.C. Pollacco, P.A. Assimakopoulos, G. Doukelis, K.G. Ioannides, D. Karadimos, D. Karamanis, M. Kokkoris, E. Kossionides, N.G. Nicolis, C. Papachristodoulou, N. Patronis, G. Perdikakis, D. Pierroutsakou, Phys. Lett. B **556**, 21 (2003).
17. M. Zadro, P. Figuera, A. Di Pietro, F. Amorini, M. Fisichella, O. Goryunov, M. Lattuada, C. Maiolino, A. Musumarra, V. Ostashko, M. Papa, M.G. Pellegriti, F. Rizzo, D. Santonocito, V. Scuderi, D. Torresi, Phys. Rev. C **80**, 064610 (2009).
18. H. Kumawat, V. Jha, B.J. Roy, V.V. Parkar, S. Santra, V. Kumar, D. Dutta, P. Shukla, L.M. Pant, A.K. Mohanty, R.K. Choudhury, S. Kailas, Phys. Rev. C **78**, 044617 (2008).
19. J.M. Figueira, J.O. Fernandez Niello, D. Abriola, A. Arazi, O.A. Capurro, E. de Barbara, G.V. Marti, D. Martinez Heimann, A.E. Negri, A.J. Pacheco, I. Padron, P.R.S. Gomes, J. Lubian, T. Correa, B. Paes, Phys. Rev. C **75**, 017602 (2007).
20. E.A. Benjamim, A. Lepine-Szily, D.R. Mendes Junior, R. Lichtenthaler, V. Guimaraes, P.R.S. Gomes, L.C. Chamon, M.S. Hussein, A.M. Moro, A. Arazi, I. Padron, J. Alcantara Nunez, M. Assuncao, A. Barioni, O. Camargo, Jr., R.Z. Denke, P.N. de Faria, K.C.C. Pires, Phys. Lett. B **647**, 30 (2007).
21. V. Morcelle, K.C.C. Pires, M. Rodriguez-Gallardo, R. Lichtenthaler, A. Lepine-Szily, V. Guimaraes, P.N. de Faria, D.R. Mendes Junior, A.M. Moro, L.R. Gasques, E. Leistenschneider, R.P. Condori, V. Scarduelli, M.C. Morais, A. Barioni, J.C. Zamora, J.M.B. Shorto, Phys. Lett. B **732**, 228 (2014).
22. A.M. Sanchez-Benitez, D. Escrig, M.A.G. Alvarez, M.V. Andres, C. Angulo, M.J.G. Borge, J. Cabrera, S. Cherubini, P. Demaret, J.M. Espino, P. Figuera, M. Freer, J.E. Garcia-Ramos, J. Gomez-Camacho, M. Gulino, O.R. Kakuee, I. Martel, C. Metelko, A.M. Moro, F. Perez-Bernal, J. Rahigh, K. Rusek, D. Smirnov, O. Tengblad, P. Van Duppen, V. Ziman, Nucl. Phys. A **803**, 30 (2008).
23. L. Acosta, A.M. Sanchez-Benitez, M.E. Gomez, I. Martel, F. Perez-Bernal, F. Pizarro, J. Rodriguez-Quintero, K. Rusek, M.A.G. Alvarez, M.V. Andres, J.M. Espino, J.P. Fernandez-Garcia, J. Gomez-Camacho, A.M. Moro, C. Angulo, J. Cabrera, E. Casarejos, P. Demaret, M.J.G. Borge, D. Escrig, O. Tengblad, S. Cherubini, P. Figuera, M. Gulino, M. Freer, C. Metelko, V. Ziman, R. Raabe, I. Mukha, D. Smirnov, O.R. Kakuee, J. Rahighi, Phys. Rev. C **84**, 044604 (2011).
24. P.R.S. Gomes, J. Lubian, I. Padron, R.M. Anjos, Phys. Rev. C **71**, 017601 (2005).
25. L.F. Canto, P.R.S. Gomes, J. Lubian, L.C. Chamon, E. Crema, J. Phys. G **36**, 015109 (2009).
26. L.R. Gasques, L.C. Chamon, D. Pereira, M.A.G. Alvarez, E.S. Rossi Jr., C.P. Silva, B.V. Carlson, Phys. Rev. C **69**, 034603 (2004).
27. L.F. Canto, P.R.S. Gomes, J. Lubian, L.C. Chamon, E. Crema, Nucl. Phys. A **821**, 51 (2009).
28. J.M.N. Shorto, P.R.S. Gomes, J. Lubian, L.F. Canto, S. Mukherjee, L.C. Chamon, Phys. Lett. B **678**, 77 (2009).
29. F. Farinon, T. Glodariu, M. Mazzocco, A. Battistella, R. Bonetti, L. Costa, A. De Rosa, A. Guglielmetti, G. Inglima, M. La Commara, V.Z. Maidikov, B. Martin, C. Mazzocchi, D. Pierroutsakou, M. Romoli, M. Sandoli, C.

Signorini, F. Soramel, L. Stroe, E. Vardaci, Nucl. Instrum. Methods B **266**, 4097 (2008).
30. E. Strano, A. Anastasio, M. Bettini, A. Boiano, C. Boiano, C. Cassese, L. Castellani, D. Corti, P. Di Meo, G. Galet, T. Glodariu, J. Grebosz, A. Guglielmetti, M. La Commara, C. Manea, M. Mazzocco, P. Molini, M. Nicoletto, C. Parascandolo, L. Parascandolo, D. Pierroutsakou, G. Pontoriere, L. Roscilli, C. Signorini, F. Soramel, L. Stroe, M. Tessaro, N. Toniolo, D. Torresi, P.G. Zatti, Nucl. Instrum. Methods Phys. Res. B **317**, 657 (2013).
31. A. Pakou, E. Stiliaris, D. Pierroutsakou, N. Alamanos, A. Boiano, C. Boiano, D. Filipescu, T. Glodariu, J. Grebosz, A. Guglielmetti, M. La Commara, M. Mazzocco, C. Parascandolo, K. Rusek, A.M. Sanchez-Benitez, C. Signorini, O. Sgouros, F. Soramel, V. Soukeras, E. Strano, L. Stroe, N. Toniolo, D. Torresi, K. Zerva, Phys. Rev C **87**, 014619 (2013).
32. Dao T. Khoa, W. von Oertzen, Phys. Lett. B **342**, 6 (1995).
33. H. De Vries, C.W. De Jager, C. De Vries, At. Data Nucl. Data Tables **36**, 495 (1987).
34. A. Bhagwat, Y.K. Gambhir, S.H. Patil, Eur. Phys. J. A **8**, 511 (2000).
35. J. Raynal, Phys. Rev. C **23**, 2571 (1981).
36. K.H. Bray, Mahavir Jain, K.S. Jayaraman, G. Lobianco, G.A. Moss, W.T.H. Van Oers, D.O. Wells, F. Petrovich, Nucl. Phys. A **189**, 35 (1972).
37. P.R. Christensen, A. Winther, Phys. Lett. B **65**, 19 (1976).
38. I.J. Thompson, M.A. Nagarajan, J.S. Lilley, M.J. Smithson, Nucl. Phys. A **505**, 84 (1989).
39. A. Pakou, N. Alamanos, N.M. Clarke, N.J. Davis, G. Doukelis, G. Kalyva, M. Kokkoris, A. Lagoyannis, T.J. Mertzimekis, A. Musumarra, N.G. Nicolis, C. Papachristodoulou, N. Patronis, G. Perdikakis, D. Pierroutsakou, D. Roubos, K. Rusek, S. Spyrou, Ch. Zarkadas, Phys. Lett. B **633**, 691 (2006).
40. Ricardo A. Broglia, Aage Winther, *Heavy Ion Reactions*, Vol. **I**: *Elastic and Inelastic Reactions* (The Benjamin/Cummings Publishing Company, Inc. 1981).
41. G.W. Fan, M. Fukuda, D. Nishimura, X.L. Cai, S. Fukuda, I. Hachiuma, C. Ichikawa, T. Izumikawa, M. Kanazawa, A. Kitagawa, T. Kuboki, M. Lantz, M. Mihara, M. Nagashima, K. Namihira, Y. Ohkuma, T. Ohtsubo, Zhongzhou Ren, S. Sato, Z.Q. Shen, M. Sugiyama, S. Suzuki, T. Suzuki, M. Takechi, T. Yamaguchi, B.J. Xu, W. Xu, Phys. Rev. C **90**, 044321 (2014).
42. D.G. Kovar, N. Stein, C.D. Bockelman, Nucl. Phys. A **231**, 266 (1974).